MICROMECHANISMS OF FRACTURE

W. Dahl*, D. Dormagen** and A. Halim*

After summarizing fracture mechanics parameters the paper briefly introduces micromechanical models of cleavage fracture and ductile crack initiation and propagation. With regard to activities of EGF-Task Group II: 'Micromechanisms' in the field of cleavage fracture different test techniques for determining the microscopic cleavage fracture stress σ_f* will be presented and the influence of notch acuity, specimen dimensions, strain rate and microstructural aspects such as grain size, carbide thickness and sulphur content/shape is discussed. The role of micromechanisms on ductile fracture initiation and propagation is outlined presenting SZW-and Δa-measurements.

INTRODUCTION

The necessity to develop high toughness materials f.i. for nuclear and offshore structures has led to an increased interest in the micromechanism of cleavage and ductile fracture and their relationships to fracture mechanics parameters such as fracture toughness K_{Ic}, J-Integral and crack-opening displacement CTOD. Moreover microstructural aspects play an important role in determination of crack initiation values and in the assessment of the scatter of results.

With regard to activities of EGF-Task Group II: 'Micromechanisms' the paper briefly presents micromechanical models to describe crack initiation and propagation under monotonic loading conditions. In the following microstructural aspects of cleavage and ductile fracture are discussed and different test techniques are presented.

* Institute for Ferrous Metallurgy of the Techn. University Aachen, W.-Germany
** Hoesch Stahl AG, Dortmund, W.-Germany

FRACTURE MECHANICS PARAMETERS

The resistance of metallic alloys to mechanical modes of crack extension is characterized by the value of fracture toughness /1/. Under linear elastic and quasi-linear elastic conditions the fracture toughness is expressed as a critical value of the stress intensity factor K_c. For extensive general yielding the crack tip region is no longer characterized by the K-dominant stress field and use can be made of critical values of the J-Integral, J_c, or the crack tip opening displacement (CTOD), δ_c. Under the conditions of small scale yielding the parameters K, J and δ are related by Eq. (1):

$$K^2 = E' J = M E' \sigma_y \delta \qquad (1)$$

where E' is Young's modulus, E, in plane stress and $E/(1-\nu^2)$ in plane strain; ν is Poisson's ratio, σ_y is the uniaxial yield stress or flow stress and M a geometrical factor, equal to unity for plane stress and approximately 2 for plane strain.

For larger amounts of plasticity the relationships in Eq. (1) are no longer valid but for exponentially hardening materials the local stresses can be related to the J-Integral according to Hutchinson /2/ and Rice and Rosengreen /3/ ('HRR-Field') and were expressed by McClintock /4/ as:

$$\sigma_{ij} = \sigma_o \left(\frac{J}{\sigma_o \varepsilon_o I_n r} \right)^{\frac{1}{n+1}} f_{ij} (\Theta, n) \qquad (2)$$

$$\text{with} \quad \frac{\sigma}{\sigma_o} = \left(\frac{\varepsilon}{\varepsilon_o} \right)^n , \quad \varepsilon_o = \sigma_o / E$$

were I_n is a parameter depending on n and loading conditions, tabulated in /4/; r,Θ are polar coordinates and f_{ij} is a function depending on Θ and n. Analogue considerations can be made for the crack tip opening displacement, when δ_t is defined as the intersection of the crack tip flanks with the 45°-line according to /5,6/

$$\delta_t = d_n J/\sigma_o \qquad (3)$$

where d_n depends on the stress state and hardening coefficient n. Beyond general yield finite element calculations indicate, that the geometrical factor M changes and depends on test piece geometry. For deeply cracked bend specimens a value of 3 is predicted in plane strain /7/. In experimental work values in the range 1 - 3 have been measured /8,9/.

At temperatures well above the ductile brittle transition, the initiation of ductile crack extension doesn't immediately lead to an unstable crack propagation or to the plastic collapse of a test piece. In this temperature regime a material's crack growth resistance curve (R-curve) is defined, where the actual values of J and δ are plotted as a function of stable crack growth Δa. The back extrapolation to the blunting-line /10/ (J_R curve) expressed by

$$J_{blunting} = 2\,\sigma_y\,\Delta a \tag{4}$$

or to a_o (δ_R-curve) /11/ enables the determination of initiation values J_{Ic}, δ_i respectively.

CLEAVAGE FRACTURE

Cleavage fracture causes new free surfaces by the rupture of atomic bonds across well defined, low index crystallographic planes. From the macroscopic point of view it is mostly a brittle type of fracture without significant plastic deformation, but providing microplasticity. In polycrystalline materials cleavage fracture is characterized by facets corresponding to the individual grains or regions of crystallographic continuity. Crack propagation accurs with high velocity mostly in a transcrystalline manner, only if the grain boundaries are segregated by impurity elements such as phosphorus, tin or antimony an intergranular type of fracture is observed.

A typical example of a cleavage fracture, characterized by cleavage facets is shown in Fig. 1. In ferritic steels fracture occurs along {100} planes.

As the local balance between fracture and yielding in bcc iron /12,13/ seems to favour yielding some form of stress intensification mechanisms must operate for cleavage to occur in steels. There is also experimental work by Low /14/ indicating that plastic flow is a necessary prerequisite to cleavage and that yielding is involved in the nucleation of cleavage fracture.

MICROSTRUCTURAL MODELS

The different models explaining the stress intensification mechanisms are discussed in detail in /15-17/ and are briefly summarized in Fig. 2.

A nucleation controlled mechanisms was suggested by Zener /18/ and Stroh /19/ such that the local stress concentration produced at the head of a dislocation pile-up could lead to cleavage fracture when the leading dislocations were squeezed together to generate a crack nucleus (see Fig. 2a).

A significant result of this model is that crack nucleation is predicted to be the most difficult stage in cleavage fracture. Therefore this model does not allow stable crack nuclei, which is in contrast to experimental observations /20/.

In steels cleavage fracture is promoted by factors producing locally elevated tensile stress levels. Cleavage of mild steels occurs at a critical tensile stress which seems to be independent of the state of hydrostatic tension /21/. This implies a propagation controlled mechanism. Cottrell /22/ proposed an alternative dislocation reaction providing for an easy nucleation in bcc metals (see Fig. 2b), by which crack nucleation will be easier than by the Zener/Stroh mechanism. This model explains the effects of grain size and yielding parameters on cleavage fracture but it neglects the possible influence of microstructural variables other than grain size.

Smith /23/ proposed a model in which a carbide particle blocks an impinging slip band (see Fig. 2c). His model predicts that the only microstructural parameter affecting the fracture stress is the carbide thickness. This disadvantage was overcome by Reiff's /24/ and Riedel's model /25/ regarding slip bands intersecting at a 90 degree angle and cracking the carbide particle. Thus the effect of grain size as well as carbide thickness, was taken into account.

DETERMINATION OF THE MICROSCOPIC CLEAVAGE FRACTURE STRESS σ_f^*

Several methods have been proposed to measure the microscopic cleavage fracture stress σ_f^*. Some of the common methods are briefly mentioned in the following and summarized in Fig. 3.

According to Orowan /26/ cleavage fracture is initiated when the fracture and the yield strength of an unnotched tensile specimen coincide

$$\sigma_f^* = \sigma_f = \sigma_y \tag{5}$$

If fracture and yield strength do not coincide Aurich /27/ suggests to set the yield strength extrapolated to 0-K equal to σ_f^*

$$\sigma_f^* = \sigma_y \ (T=0K) \tag{6}$$

In order to avoid tests at extremely low temperatures notched bend or tensile specimens can be used when the stress distribution ahead of the notch is known. Then the maximum tensile stress is considered to be equal to σ_f^*:

$$\sigma_f^* = \sigma_{yy}^{max} \tag{7}$$

The maximum local tensile stress can be calculated by Hill's slip line field theory at general yield temperature

$$\sigma_{yy} = \sigma_y \left(1 + \frac{\pi - \omega}{2}\right) = \sigma_y \, k_{pl}^{max} \tag{8}$$

where σ_y is the materials yield strength, ω is the notch angle and k_{pl} is the plastic stress concentration factor.

Finite element calculations of the stress distribution can lead to better results, because the material work hardening behaviour can be taken into account. Moreover Dahl et al /28/ have demonstrated a more pronounced effect of notch root radius rather than the notch angle. Another advantage of FE-calculation is the use of a normalized stress concentration

$$\sigma_{yy}/\sigma_y = \sigma_N/\sigma_y \tag{9}$$

with σ_N = net section stress

which allows to determine σ_f^* as a function of temperature, whereas Eq. (8) can only be used at general yield temperature.

Ritchie, Knott and Rice /29/ have modified Eq. (7) by introducing a critical distance x_c across which σ_f^* must be exceeded:

$$\sigma_f^* = \sigma_{yy}\,(x_c) \tag{10}$$

This fracture criterion is based on the idea that cleavage fracture is propagation controlled.

Recently Wallin et al /30/ have introduced a statistical fracture model which takes into account the carbide size distribution: According to Curry and Knott /31/ the Griffith crack advancement criterion for a round carbide has the form of Eq. (11) and is used as a fracture criterion

$$\sigma_f^* = \left\{ \frac{\pi \; E\,(\gamma_s + w_p)}{2\,(1 - \nu^2)\, r_o} \right\}^{1/2} \tag{11}$$

where ν is Poisson's ratio, γ_s the surface energy, w_p is the plastic work necessary for crack propagation and r_o is the radius of the fractured carbide. Fracture is assumed to occur when the tensile stress σ_{yy}:

$$\sigma_{yy} = f\,(\sigma_y,\ x,\ K_I,\ n,\ E)$$

ahead of a crack tip at the site of a carbide having a radius of r_o exceeds $\sigma_f{}^*$ given by Eq. (11).

Within the EGF-Task Group II 'Micromechanisms' a Round-Robin has just been initiated to compare the different evaluation methods of the microscopic cleavage fracture stress $\sigma_f{}^*$. Six laboratories (besides from W.-Germany, also from United Kingdom, Finland and France) intend to join this RR. The slip line field theory, FE-calculations and the statistical fracture approach will be compared among each other, using a mild steel C10 with simple microstructures.

In the following some influencing parameters on the microscopic cleavage fracture stress $\sigma_f{}^*$ will be discussed. $\sigma_f{}^*$ was determined by the combination of experiments on double edge notched tensile specimens and elastic-plastic FE-calculations to evaluate the stress distribution. The method is shown in Fig. 4. The RKR-criterion (Eq. (11)) was used to calculate $\sigma_f{}^*$. The value of x_c was fitted such that $\sigma_f{}^*$ becomes independent of temperature and geometry /32/.

Influence of testing parameters.

The influence of work hardening on the stress distribution ahead of a notch is shown in Fig. 5. For the mild steel C 75 the stress ratio σ_{yy}/σ_y is plotted versus the distance from notch root for different notch angles and notch radii. Elastic-plastic finite element solutions (plane strain) are compared with slip line field theory. There is a good agreement between the two methods between notch root and that point, where the σ_{yy}^{max}-value is reached. The greatest deviation occurs at the notch root for high stresses, due to work hardening and in the region of the maximum. The differences in the maximum values of stress concentration of FE- and SL-results may be explained by the spread of the plastic zone not only in form of logarithmic spirals in front of the notch - as predicted by SL-theory - but also in form of wings somewhat above the ligament. In Fig. 6 the fracture criteria given by Eqs. (8) and (10) are compared among each other. In both cases a FE-analysis was used to determine $\sigma_f{}^*$ for the steel C 10. For the maximum tensile stress σ_{yy}^{max} there is a strong influence of notch radius, the values of smaller radii being significantly higher, and below the temperature, where general yielding occurs (T_{gy}) there is nearly no influence of temperature. The different series are characterized by the notch angle and the notch radius e.g. 253 stands for a 30° notch angle and a radius of 0.25 mm. Assuming a critical distance value x_c of 0.1 mm results in a microscopic cleavage stress $\sigma_f{}^*$ being independent of notch acuity and temperature. Above the transition temperature where general yielding is observed there is still a decrease in fracture stress with increasing temperature. The mean ferrite grain diameter was determined to d_m = 43 μm. Thus the experimental results, the critical distance x_c being twice the grain diameter are in good agreement with theoretical predictions /29/.

The influence of loading rate on the microscopic cleavage stress is shown in Fig. 7. For the mild steel C 10 with d_m = 90 μm cleavage fracture stress is plotted as a function of temperature /33/. Assuming a critical distance x_c of 0.15 mm there is no influence of strain rate by changing the cross head speeds from q = 1 mm/min to 100 mm/min.

Influence of metallurgical parameters.

It is found experimentally that σ_f^* increases with a decrease in grain size /31,32,34/ (see Fig. 8). This is in good agreement with the models presented by Cottrell, Reiff and Riedel but not predicted by Smith's model of microcrack propagation, which suggests that σ_f^* should depend only on carbide thickness. From this model the increase of σ_f^* with decreasing grain size seems to occur because carbide thickness and grain size are interrelated in steels which have been simply cooled from austenite, so that fine grains are associated with fine carbides. The influence of carbide thickness independently of grain size is shown in Fig. 9. Decreasing the carbide thickness from 2 - 3 μm to 0.5 μm results in an increase of microscopic cleavage stress from 1100 MPa to 1300 MPa for the mild steel C 10 with a grain size of 22 μm.

The effect of prestraining is important for practical purpose, too. After prestraining an increase in σ_f^* is observed in literature /33,35,36/ (see Fig. 10). The increase of dislocation density leads to an increase of free dislocations so that - according to Smith's theory - stresses ahead of carbide particles are reduced.

The influence of sulfur content and sulfur shape is demonstrated in Fig. 11 for the steels Fe 510 and Fe E 350 /37/. Within the range from 0.002 % S to 0.019 % S no influence of sulfur content and sulfur shape caused by different desulfurisation techniques on σ_f^* is to be observed. For 125 mm - thick plate of Fe E 350 tested in the TL-, LT- and ST-orientation the missing influence of sulfur shape on the microscopic cleavage fracture stress is affirmed. For both materials an influence of grain size on σ_f^* can be excluded, because the grain size was constant. These results are in contrast to recent experiments of Bowen and Knott /38,39/ who found for an A533B steel a significant influence of sulfide inclusions on the microscopic cleavage fracture stress. Lower σ_f^* values were measured in the ST-orientation. These contradictions needs further discussion.

CORRELATION BETWEEN FRACTURE TOUGHNESS AND MICROSCOPIC CLEAVAGE FRACTURE STRESS

As the stress field ahead of a crack is described by the stress intensity factor K according to

$$K = \sigma_{(r)} \, (2\pi r)^{1/2} \tag{12}$$

where $\sigma_{(r)}$ is the stress at distance r, the fracture process can be described by

$$K_{Ic} = \sigma_f^* \, (2\pi r^*)^{1/2} \tag{13}$$

if a single microcrack were located at the position r^*. Of course Eq. (13) is an oversimplification, but by introducing the RKR-criterion (Eq. (10)) a statistical average representing the probability of finding a carbide of representative thickness at a given distance ahead of the crack tip can be assumed.

Using the RKR-model it is possible to predict the fracture toughness as a function of temperature, assuming constant values of σ_f^* and x_c, if the temperature dependence of the yield stress is known and the stress distribution for crack tip behaviour according to Tracey /40/ in small scale yielding is used.

For two different heat treatments of the steel 20 MnMoNi 55 measured and predicted K_{Ic} values are compared in Fig. 12a in a temperature range from 77 K up to 240 K /41/. There is a good agreement within the regime of linear elastic fracture mechanics, and the results demonstrate that different types of specimens (CT- and CCP type) fail by cleavage, when the maximum tensile stress exceeds the microscopic cleavage stress σ_f^* across a critical distance x_c.

With increasing plasticity the influence of crack tip blunting on the stress field ahead of the crack is no longer neglegible. Schmidtmann and Nierhoff /42/ have modified Eq. (10)

$$\sigma_f^* = \sigma_{yy} \, (x'_c) = \sigma_{yy} \, (R_c + x_c) \tag{14}$$

where due to crack tip blunting R_c is the critical distance from the notch tip to the fracture process zone described by x_c. By combining the increase of stresses ahead of a notch given by slip line field theory and FE-calculations the fracture toughness can be calculated by

$$K_{Ic} = \sigma_y \left(\frac{x_c}{f\left(\frac{\sigma_f^*}{\sigma_y}\right) - \frac{\sigma_y}{2\,E'\,\beta}\left[\exp\left(\frac{\sigma_f^*}{\sigma_y} - 1\right) - 1\right]} \right)^{1/2} \qquad (15)$$

were $f(\sigma_f^*/\sigma_y)$ is the FE-stress distribution without crack tip blunting and β is a factor depending on the stress state.

The application of Eq. (15) is shown in Fig. 12b for the steel Fe 510 + CaSi which demontrates a good agreement between measured and predicted K_{Ic}-values /43/.

DUCTILE FRACTURE

Void Nucleation and Coalescence

Above the transition temperature, microcracks do not propagate by cleavage but the crack advance proceeds by the coalescence of voids centred on non-metallic inclusions or other second-phase particles /36/. At low plastic strains the inclusions decohere from the matrix and smaller microvoids can be nucleated by grain boundary carbides (of approx. 1 µm diameter). When the load applied to a testpiece is increased, voids are produced by the high plastic strains ahead of the precrack and expand under the combination of local stress field and hydrostatic stress component. Crack 'initiation' is defined as the point at which the blunting precrack coalesces with a growing void. The initiation value of stable crack growth δ_i is measured at the position of the original crack tip (see Fig. 13).

Based upon the void growth model of Rice and Tracey /44/ which describes the growth of a spherical void in a non-hardening material

$$\frac{dR}{d\bar{\varepsilon}} = 0{,}28\ R\ \exp\,(3\sigma_m/2\bar{\sigma}) \qquad (16)$$

where R is the radius of the void, $d\bar{\varepsilon}$ the increment of equivalent strain, σ_m the mean stress and $\bar{\sigma}$ the equivalent stress, much experimental and theoretical investigations have been performed to describe the complexity of ductile fracture characterized by void nucleation, growth and coalescence /45-48/.

From these predictions two conclusions may be drawn. Firstly initiation values of fracture toughness may be increased by ensuring that inclusions are small and widely spaced. This is easily achieved in steels with low sulfur content and sulfur shape control /49/. As weld metal, in particular, may contain a high volume fraction of closely-spaced silicates, acting as void initiator, δ_i values can be lower than for the parent steel, but for multi-pass submerged arc weldings under optimized welding conditions δ_i-values may also be even better than for the parent metal /50/. Secondly the specimen orientation will influence elastic-plastic fracture toughness data, due to the shape of sulfides elongated by the rolling process /51,52/, resulting in lower toughness values for crack initiation and crack propagation especially in the S-L direction. Experimental results are usually carried out on axi-symmetric notched tensile specimens, which allow measuring the failure strains as a function of stress state parameter. An example is given in Fig. 14 where the equivalant failure strain is plotted as a function of stress state parameter $\sigma_m/\bar{\sigma}$ for steel FeE 350 in LT-, TL-, and SL-orientation. These experimental results can be inserted in FE-calculations, as recently described by Rousselier et al /53/, which allow the safety assessment of a cracked body concerning crack initiation and propagation based upon microstructural values.

Besides of this very interesting and promising progress the activities in the field of ductile fracture within in the TG II have concentrated on the reliabability and reproducebility of microstructural aspects concerning the determination of macroscopic values for crack initiation, especially crack growth- and 'stretch-zone' measurements, partly to understand the scatter of experimental results from a microscopic point of view.

Within the Task Group 'Micromechanisms' one RR on crack growth measurements is almost completed on specimens which were used in a RR on crack initiation methods within the Task-Group 'Elastic-Plastic- Fracture Mechanics' and a second RR on 'SZW' measurements has just been initiated. The aim of both round robins were to evaluate the scatter concerning microstructural aspects of ductile fracture by comparing different test techniques.

In Fig. 15 the results of the German participants in the EGF-RR are presented. The mean values of Δa determined after the procedure given by ASTM E 813 are compared between direct (travelling microscope) and indirect (Photos) measurements. The agreement between both techniques is good, independent of the absolute amount of stable crack extension. Compared with the mean values the scatter of the single located measuring points ($1 \leq i \leq 9$) is more pronounced as demonstrated in Fig. 16 where for a ductile steel Fe E 350 the median value $\Delta\tilde{a}_i$, is plotted versus the mean value $\Delta\bar{a}_i$. It is surprising that the measuring points located in the mid-thickness position exhibit the most pronounced scatter which is caused by an excessive local crack advance. Moreover the specimen without side-grooves show a reduction of thickness which makes the exact positioning of the single locations more difficult especially as precise prescriptions are missing in the standards.

Combining the results of the German participants of the EGF- RR and the RR in the German fracture group one can see that the uncertainty in the determination of stable crack length is at least ± 10 %. This is demonstrated in Fig. 17, where the standard deviation is plotted as a function of stable crack growth Δa for different steels. As the standard deviation increases with increasing Δa, one has to claim that the calibration of indirect crack growth measurements like potential drop or unloading compliance technique should be done at small amounts of stable crack growth.

This uncertainty in the Δa-measurement can lead to a scatter of ± 10 % in the J_{Ic}-determintation, as demonstrated in Fig. 18 independent of the procedure chosen. In this figure the ASTM standard is compared with the Loss-, the Neale and the DVM- procedure. The latter was proposed by a working group within the German fracture group. The last three proposals are being discussed thoroughly in the EGF- TG I Elastic-Plastic Fracture Mechanics.

A second aspect where micromechanisms play an important role is the determination of crack initiation values with the aid of 'stretch-zone' width (SZW-) measurement. On this topic a Round Robin was just initiated amongst 13 participants (Table 1) in order to check this method concerning the applicability and the scatter of the results. The aim of this RR is to check the influence of specimen geometry, stress state and different test techniques on SZW-measurement.

It was recently shown by Sun et al /54/ that SZW-measurement is a useful method to determine physical initiation values, which are lower then those determinded by the ASTM-standard (see Fig. 19).

Especially the generalized ASTM-blunting line, calculated by

$$J = 2\, \sigma_{fl}\, \Delta a \tag{17}$$

seems not to be appropriate for ductile materials, as shown in Fig. 20, where the calculated, measured (SZW) and theoretical (HRR-Field) blunting behaviour is compared. SZW-measurements and HRR-Field calculation are in good agreement for Fe 510 and 42 CrMo 4 steel, whereas the ASTM proposal overestimates the material blunting-behaviour /55/. Similar results were obtained by a Round Robin within the German Fracture Group (DVM-Kennwertermittlung) /56/.

Future work should also concentrate on ductile failure criterion, as already shown in Fig. 14, because these microscopic aspects can also be used in Finite-Element-calculations. This is already used by the French Group and seems to be an interesting alternative to the macroscopic description of the failure of a structure.

SYMBOLS USED

c	critical (as Index)
CTOD	crack tip opening displacement
d	grain size
d_n	constant, which depends on the stress state and hardening exponent n
D	carbide thickness
E'	Young's modulus
f_{ij}	known dimensionless functions of the circumferential position Θ and the hardening exponent n
I_n	constant, which is a function of n
J	J-integral
K	stress-intensity factor
K_{Ic}	fracture toughness
k_{pl}	plastic stress concentration factor
M	$1/d_n$
n	strain hardening exponent
r	distance for fracture process, polarcoordinate
r_o	radius of the fractured carbide
r^*	critical distance
R	radius of void
T_{gy}	temperature at general yield
T_i	temperature at crack initiation
w_p	plastic work
β	constant
γ_s	surface energy
δ	crack opening displacement
ε	strain
ε_o	reference strain
$\varepsilon_{ij}, \sigma_{ij}$	local tensile strain, stress
σ	stress
σ_o	reference stress
σ_f	fracture stress

σ_f^*	microscopic cleavage fracture stress
σ_{fl}	flow stress
σ_N	net section stress
σ_y	yield stress
τ_i	shear stress
τ_{eff}	effective shear stress
Θ	polarcoordinate
ω	notch angle

REFERENCES

/1/ Schwalbe, K.H.,
K. Hansen Verlag, München, Wien 1980

/2/ Hutchinson, J.W.,
J. Mech. Phys. Solids 16 (1968), p 337/47

/3/ Rice, J.R. and G.F. Rosengreen
J. Mech. Phys. Solids 16 (1968), p. 1/13

/4/ Mc Clintock, F.A.
in: Fracture Vol. III, Ed. H. Liebowitz, New York 1971,
p. 48/225

/5/ Shih, C.F.: General Electric Company
TIS Report No 79 CRC075, 1979

/6/ Rice, J.R. and D.M. Tracey, In: Numerical and Computer
Methods Structural Mechanics, S.J. Feuves et al. Eds,
Academie Press, New York, 1973, S. 585/623

/7/ McMeeking, R.M. and D.M. Parks
ASTM STP 668 (1979) p. 175/95

/8/ Willoughby, A.A. Ph.D-thesis, Imperial College, London 1979

/9/ Slatcher, S., Ph.D-thesis, University of Cambridge, 1983

/10/ ASTM E 813, Annual Book of ASTM Standards, Part 10
Americal Society of Testing and Materials, Philadelphia Pa,
1981

/11/ Methods for Crack Opening Displacement Testing BS 5762,
British Standard Institution, Londond 1979

/12/ Kelly, A., Tyson, A. and Cottrell, A.H.
Philos. Mag. 15 (1967), p. 567

/13/ Rice, J.R. and Thomson, R.
"Ductile Versus Brittle Behaviour of Crystals" (1974), p. 73

/14/ Low, J.R.
Trans. ASM 46 A (1954), p. 163

/15/ Curry, D.A.
Met. Sci. 14 (1980), p. 319/28

/16/ Knott, J.F. in: "Application of Fracture Mechanisms to Materials and Structures (AFMMS)", Freiburg-FRG, 1983
Eds. G.C. Shih, E. Sommer and W. Dahl

/17/ Dahl, W. and D. Dormagen in "Elastic Plastic Fracture Mechanics", 1985, ECSC, EEC, EAEC, Brussels and Luxembourg, p. 203/25

/18/ Zener, C.
ASM 40 (1948), p. 3/31

/19/ Stroh, A.N.
Proc. Roy. Soc. A 223 (1954), p. 404/14

/20/ Hahn, G.T., Averbach B.L., Owen, W.S. and Cohen, M.
Proc. Int. Conf. on Atomic Mechanisms of Fracture, Swamscott (1959), p. 91/116

/21/ Knott, J.F.
J. ISI 204 (1966), p. 104/11

/22/ Cottrell, A.H.
Trans. AIME 212 (1958), p. 192

/23/ Smith, E.
Proc. Conf. Physical Basis of Yield and Fracture, Oxford, Inst. Phys. and Phys. Soc., London 1966, p. 36

/24/ Reiff, K.H.
Arch. Eisenhüttenwes. 43 (1972), p. 567/70

/25/ Riedel, H. and Kochendörfer, A.
Arch. Eisenhüttenwes. 50 (1979), p. 173/8

/26/ Orowan, E.
Rep. Prog. Phys. 12 (1948), S. 185/232

/27/ Aurich, D. and Wobst, K.
Arch. Eisenhüttenwes. 52 (1981), p. 202/8

/28/ Kühne, K., Redmer, J. and Dahl, W.
Eng. Fract. Mech. 16 (1982), p. 845/55

/29/ Ritchie, R.O., Knott, J.F. and Rice, J.R.
J. Mech. Phys. Solids 21 (1973), p. 395/410

/30/ Wallin, K., Saario, T., Torrönen, K. and Forsten, J.
"A microstatistical model for carbide induced cleavage fracture", Res. Rep., Techn. Res. Centre of Finnland, 1983

/31/ Curry, D.A. and Knott, J.F.
Met. Sci. 12 (1978), p. 511/4

/32/ Kühne, K., Ph.D-Thesis, RWTH Aachen-FRG, 1982

/33/ Dahl, W., Uebags, M. and Kühne, K.
Arch. Eisenhüttenwes. 48 (1977), p. 541/5

/34/ Dahl, W. and Uebags, M.
Stahl und Eisen 97 (1977), p. 486

/35/ Groon, J.D.G. and Knott, J.F.
Met. Sci. 9 (1975), p. 390/400

/36/ Sandström, R., Engbert, G. and Bergström, G.
Met. Sci. 10 (1976)

/37/ Dormagen, D., Ph.D-Thesis, RWTH Aachen-FRG, to be published 1986

/38/ Bowen, P. and Knott, J.F.
Met. Sci. 18 (1984), p. 225/35

/39/ Bowen, P. and Knott, J.F.
J. of Fract. 28 (1985), p. 103/17

/40/ Tracey, D.M.
J. Engng. Mat. Techn. (1976), p. 145/51

/41/ Dormagen, D., Dahl, W. and Dünnewald, H.
in: "Advances in Fracture Research" (ICF6), Eds. S.R. Valluri et al, New Delhi (1984), Vol. 2, p. 803/9

/42/ Schmidtmann, E. and Nierhoff, H.
Arch. Eisenhüttenwes. 50 (1979), p. 161/6

/43/ Halim, A., Dormagen, D., Dünnewald-Arfmann, H., Twickler, M., Twickler, R. and Dahl, W.
will be presented in "International Seminar on Local Approach of Fracture", France, 1986

/44/ Rice, J.R. and Tracey, M.A.
J. Mech. Phys. Solids (1969), p. 201/17

/45/ Hancock, J.W. and Mackenzie, A.C.
J. Mech. Phys. Sol. 24 (1976), p. 147/69

/46/ King, J.E., Smith, R.F. and Knott, J.F.
in: "Fracture 1977", Proc. 4th Int. Cong. on Fracture ed.
D.M.R. Taphir, Press Perganon, 2 (1977), p. 357

/47/ Henry, J., Marandet, B., Mudry, F. and Pineau, A.
IRSID Rep. Nr. P E 3843 BM/CR, 313518, RE 1133, Oct. 1984

/48/ Devaux, C.J.
presented at the "Meeting of The France Fracture Group"
1984, Florance, France

/49/ Green, G.
presentend at "Forth Europeas Congress on Fracture",
Loeben, 1982

/50/ Schmitz-Cohnen, K.
Ph.D-Thesis, RWTH Aachen FRG, to be published 1986

/51/ Dormagen, D. and Dahl, W.
Int. Conf. of Appl. of Fract. Mech. To Mat. and Struc.
(AFMMS), 1983

/52/ Hancock, J.W. and Cowling, M.J.
Met. Sci. 14 (1980), p. 293/304

/53/ Rousselier, G., Devaux, C.J. and Mottet, G.
in: 'Advances in Fracture Research' (ICF 6), Eds. S.R.
Valluri et al, New Delhi (1984), Vol. 2, p. 1205/13

/54/ Sun, D.-Z., Dormagen, D. and Dahl, W.
Steel Research 8 (1985), p. 445/9

/55/ Sun, D.-Z., Dormagen, D. and Dahl, W.
to be published in ECF 6, Amsterdam

/56/ Heerens, J., Cornec, A. to be published

Laboratory	Technique					
	Participant	Photo	SEM	Infiltration	Stereophoto	Microscope
1) Harewell, UK	1	x				
2) The Welding Institute, UK	1	x	x			x
3) DNV, Norway	1	x	x			
4) EIR, Switzerland	1	x	x			
5) University of Leoben, Austria	1	x	x		x	
6) MPI, FRG	1	x	x			
7) GKSS, FRG	1	x	x	x		
8) BAM, FRG	1	x	x			
9) Politecnico Torino, I	1	x	x			
10) IEHK, FRG	3	x	x			
11) EMV, Switzerland	1	x	x			
12) KFK, Karlsruhe, FRG	1	x	x			
13) KWU, AG, FRG	1	x	x			

Table 1 The list of participants and their test equipment

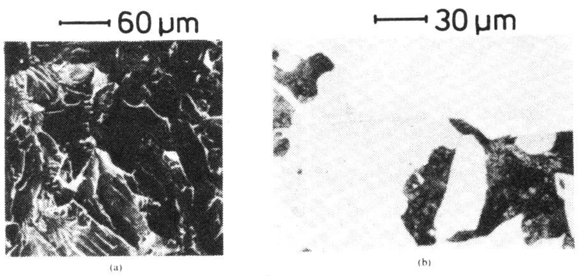

Fig. 1 Cleavage facets in mild steel

a) fracture surface b) section through nickel plated fracture surface

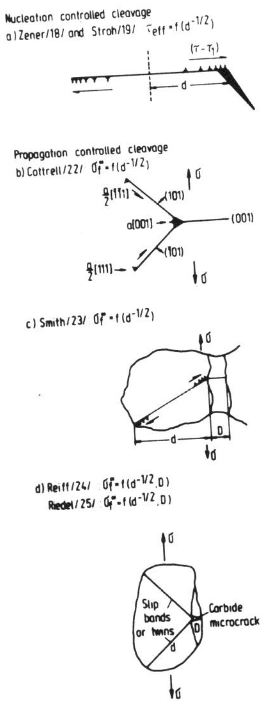

Fig. 2 Model of cleavage fracture process

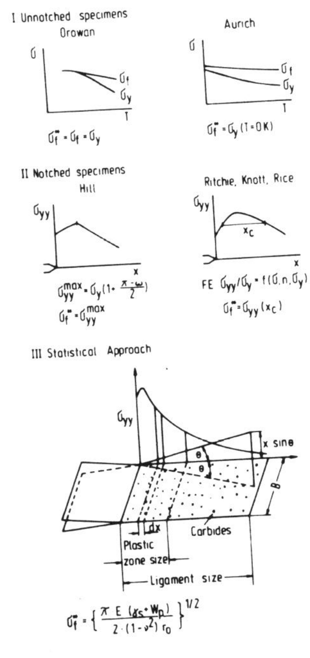

Fig. 3 Determination of σ_f^*

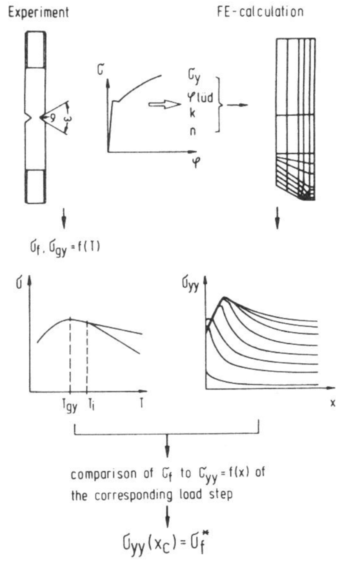

Fig. 4: Scheme for determining σ_f^*

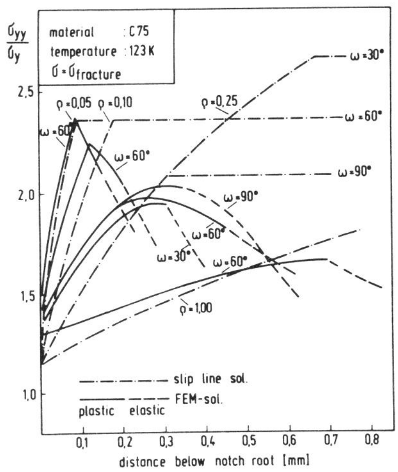

Fig. 5: σ_{yy} stress distribution ahead of the notch root at fracture load for different notch geometries /28/

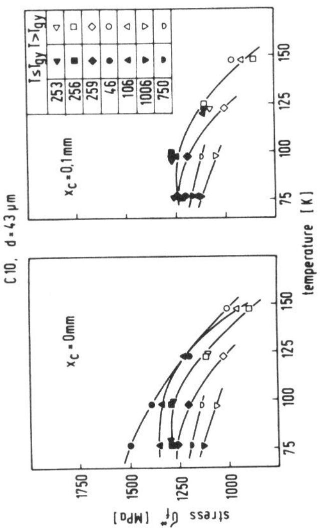

Fig. 6: Influence of notch acuity on $\sigma_f^* = f(T)$ /32/

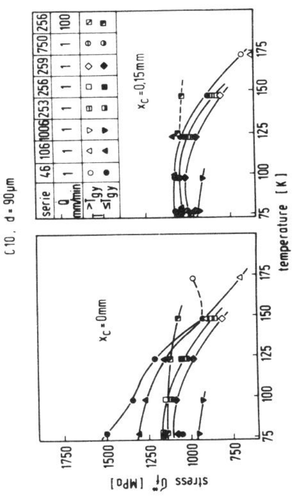

Fig. 7: Influence of loading rate on $\sigma_f^* = f(T)$ /33/

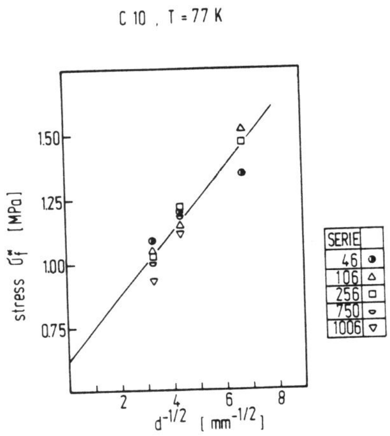

Fig. 8: Grain size dependence of σ_f^*

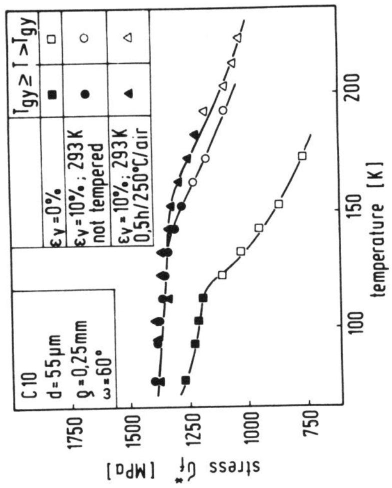

Fig. 9: Influence of carbide thickness on σ_f^* /29/

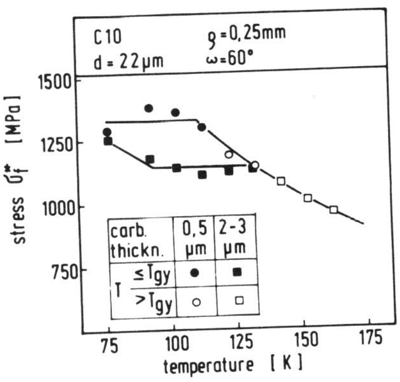

Fig. 10: The effect of prestraining on σ_f^*

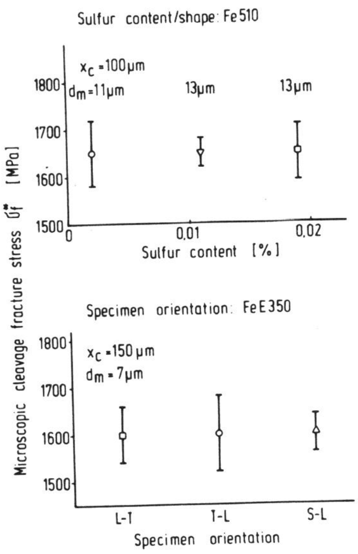

Fig. 11: Influence of sulphur content and sulphur shape on σ_f^*

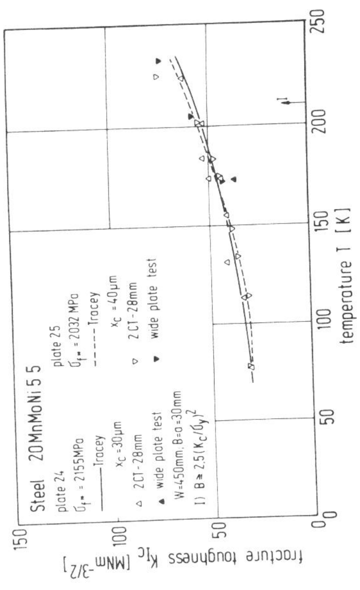

Fig. 12a: Correlation between K_{Ic} and σ_f^* for steel 20 MnMoNi 5 5 /41/

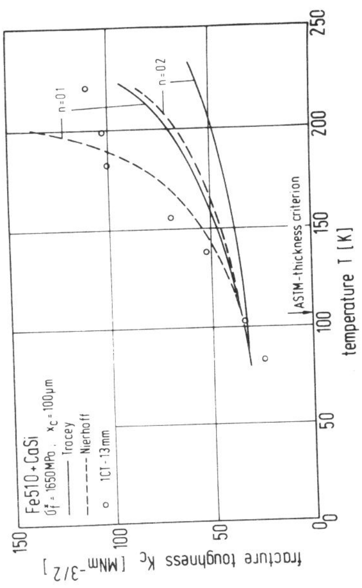

Fig. 12b: Correlation between K_c and σ_f^* for steel Fe 510 + CaSi /43/

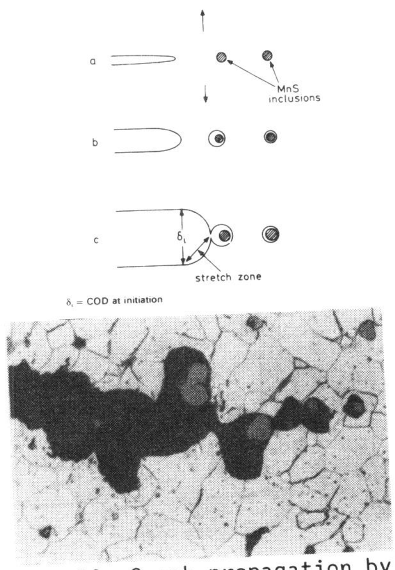

Fig. 13: Crack propagation by void coalescence

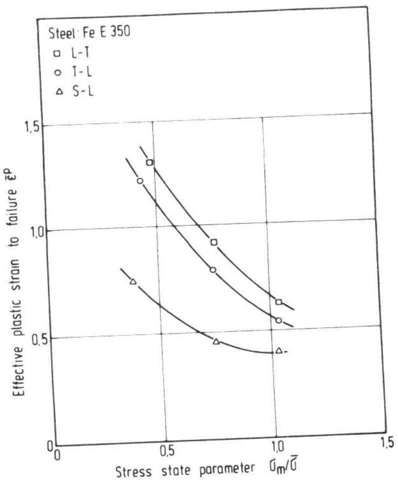

Fig. 14 Effective plastic strain to failure $\bar{\varepsilon}^p$ as a function of stress state parameter $\sigma_m/\bar{\sigma}$

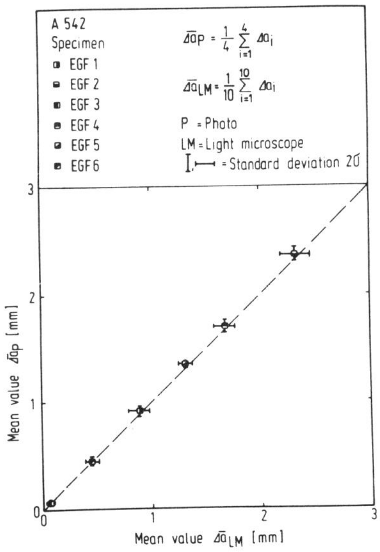

Fig. 15: Comparison of Δa-values, determined from light microscope and photo

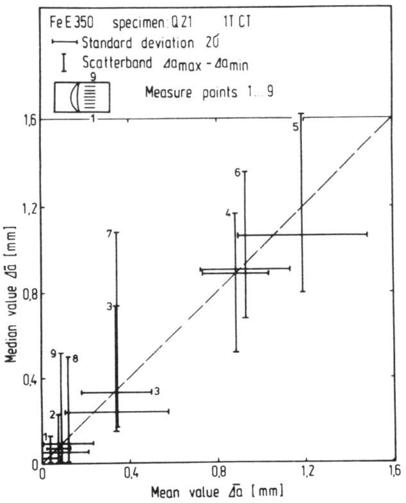

Fig. 16: Scatter of the single measure points 1 to 9 of the specimen Q 21

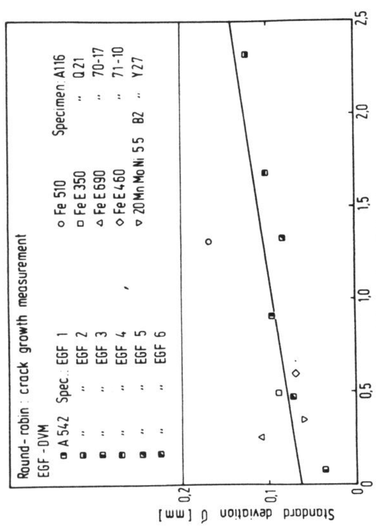

Fig. 17 Scatterband of Δa values of EGF and DVM Round Robin

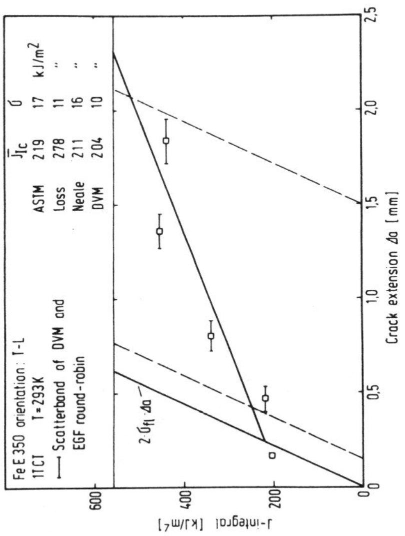

Fig. 18 Scatter of the J_{Ic}-values for different evaluation procedures for steel Fe E 350

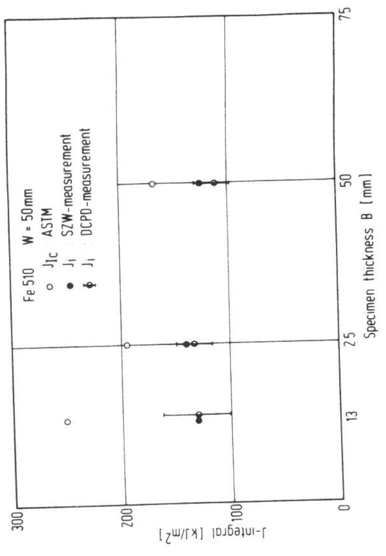

Fig. 19: Influence of specimen thickness on different crack initiation values

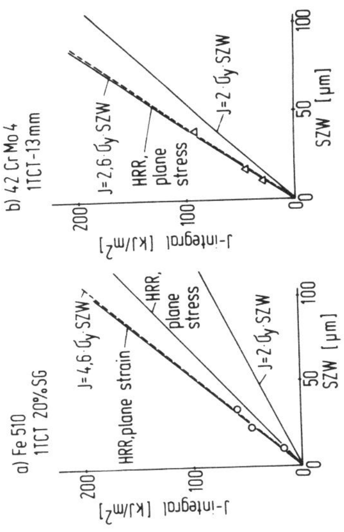

Fig. 20: Comparison between calculated and experimentally determined blunting behaviour for a) Fe 510 and b) 42 CrMo 4